Eur. Phys. J. B (2014) 87: 77
DOI: 10.1140/epjb/e2014-50017-5

THE EUROPEAN PHYSICAL JOURNAL B

Regular Article

Reaction-diffusion scheme for the clock and wavefront mechanism of pattern formation

Piotr Dziekan[1,2,3,a], Bogdan Nowakowski[1,4], and Annie Lemarchand[2,3]

[1] Institute of Physical Chemistry, Polish Academy of Sciences, Kasprzaka 44/52, 01-224 Warsaw, Poland
[2] Sorbonne Universités, UPMC Univ. Paris 06, Laboratoire de Physique Théorique de la Matière Condensée (LPTMC), 4 place Jussieu, case courrier 121, 75252 Paris Cedex 05, France
[3] CNRS UMR 7600, LPTMC, 75252 Paris, France
[4] Physics Laboratory, Warsaw University of Life Sciences - SGGW, Nowoursynowska 159, 02-776 Warsaw, Poland

Received 8 January 2014 / Received in final form 18 February 2014
Published online 1st April 2014

Abstract. We present a model of pattern formation in reaction-diffusion systems that is based on coupling between a propagating wave front and temporal oscillations. To study effects of internal fluctuations on the spatial structure development we use a chemical master equation for our reaction-diffusion model. First, a model with local, uncoupled oscillators is studied. Based on it we show that synchronization of oscillations in neighboring cells is necessary for the formation of regular patterns. We introduce synchronization through diffusion, but then, to get a stable pattern, it is necessary to add an additional species that represents the local state of the system. Numerical simulations of the master equation show that this extended model is resistant to fluctuations.

1 Introduction

Nonlinear reaction-diffusion systems in conditions out of equilibrium are known to produce stable spatial structures. The principal example of this behavior are Turing patterns, which are formed in activator-inhibitor systems if mobilities of species are different [1–3]. This mechanism can explain formation of many shapes observed in nature, most notably animal coat patterns [4–6].

In this paper we present a different type of generic reaction-diffusion scheme that can produce stable, periodic structures. It is inspired by the ideas of Cooke and Zeeman, who proposed a clock and wavefront model as a mechanism of axial segmentation during embryonic development [7]. Spatial patterns in the Belousov-Zhabotinsky reaction were produced in an experiment based on the clock and wavefront mechanism [8].

The concept is that the whole system undergoes temporal, in-phase oscillations. At one point, a wave front starts propagating from a boundary. This wave front arrests oscillations, i.e. upon front arrival, they are stopped and local state of the system develops to one of the two stable stationary states, depending on the phase of the oscillator. This gives rise to a spatial pattern with period equal to the distance covered by the wave front during one period of temporal oscillations. To prevent the final structure, consisting of alternating regions in different stable states, from developing to homogeneous state, some of the species of the scheme have to be immobile.

Many authors have studied the problem of synchronization of oscillations [9–13]. The need of synchronization of oscillations in our model is dicussed. Section 2 contains the design of a model with a wave front coupled to chemical oscillators and without synchronization of oscillations in spatial cells. Consequences of lack of synchronization are examined by numerically solving the master equation. An extended model including diffusive coupling between molecular clocks is presented in Section 3 and its robustness with respect to internal fluctuations is discussed. Conclusions are given in Section 4.

2 Model without coupling of oscillators

We want to develop an as simple as possible reaction-diffusion scheme that would correspond to the clock and wavefront mechanism of pattern formation. The proposed scheme is composed of two elements, one dedicated to the wave front of antagonistic concentrations and the other to temporal oscillations. Various types of wave fronts exist, which can expand between stable or unstable stationary states [14]. We choose a trigger wave, which propagates between regions in which the system is in two different stable stationary states. It involves two species denoted by A and P. The species A reacts according to the Schlögl scheme [15], which is the simplest bistable model involving

[a] e-mail: pdziekan@ichf.edu.pl

a single species of variable concentration:

$$2\mathrm{A} + \mathrm{R} \underset{k_{-1}^{f}}{\overset{k_1^{f'}}{\rightleftarrows}} 3\mathrm{A}, \tag{1}$$

$$\mathrm{A} \underset{k_{-2}^{f'}}{\overset{k_2^{f}}{\rightleftarrows}} \mathrm{R}, \tag{2}$$

where $k_1^{f'}$, k_{-1}^{f}, k_2^{f} and $k_{-2}^{f'}$ are rate constants. The concentration of R species is considered to be constant. For simplicity, different species that act as a reservoir will be denoted by R in the following. To obtain concentration of P antagonistic to that of A, we assume that A catalyses degradation of P that is counterbalanced by production of P from R:

$$\mathrm{P} + \mathrm{A} \xrightarrow{k_3^{f}} \mathrm{R} + \mathrm{A}, \tag{3}$$

$$\mathrm{R} \xrightarrow{k_4^{f'}} \mathrm{P}. \tag{4}$$

Reaction-diffusion equations, which govern evolution of concentrations A and P of the two species related to the wave front, are given by:

$$\partial_t A = -k_{-1}^{f} A^3 + k_1^{f} A^2 - k_2^{f} A + k_{-2}^{f} + D_A \partial_{xx} A, \tag{5}$$

$$\partial_t P = -k_3^{f} AP + k_4^{f} + D_P \partial_{xx} P, \tag{6}$$

where $k_1^{f} = k_1^{f'} R$, $k_{-2}^{f} = k_{-2}^{f'} R$ and $k_4^{f} = k_4^{f'} R$. For the chosen parameter values, dynamics admits two stable stationary states (A_-, P_+) and (A_+, P_-), with $A_- < A_+$ and $P_- < P_+$. In the following, the $-$ and $+$ indices are attributed to the steady states of lower and higher concentrations of a couple of given species, respectively.

We assume that initially, small region close to the axis origin is in the steady state (A_+, P_-) and the remaining part is in the steady state (A_-, P_+). For the chosen parameter values, a wave front propagating in the positive direction develops as shown in Figure 1. An analytical expression for front propagation speed in the Schlögl model is

$$v_f = \sqrt{\frac{k_{-1}^{f} D_A}{2}} (A_- + A_+ - 2A_u), \tag{7}$$

where A_u is the middle root of equation (5), i.e. the value of A in the unstable stationary state.

Next we introduce the second element of the model, the molecular clock. Nonlinear reactions between at least two species of variable concentrations can result in a limit cycle attractor in the phase space, i.e. in temporal oscillations of concentrations. We start with the scheme of the Brusselator model [16], which includes two types of molecules X and Y and was designed to illustrate periodic oscillations. We modify this scheme to obtain an arrest of oscillations upon wave front arrival.

The wave front is supposed to switch the (X, Y) dynamics from oscillatory regime to bistable regime [17]. To introduce coupling between the wave front and the clock, we postulate that A and P species catalyse some

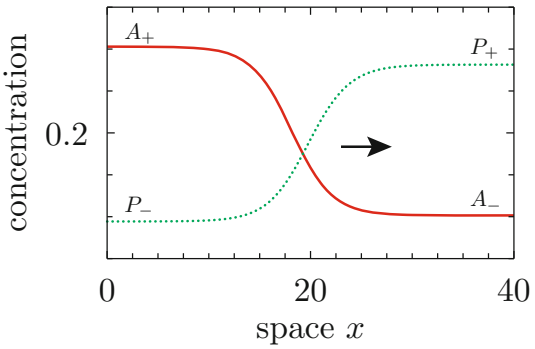

Fig. 1. Wave front of species A and P. Shape of the wave front obtained from numerical integration of reaction-diffusion equations given in equations (5) and (6). Concentration of A is plotted with solid line and concentration of P, with dotted line. Axis origin is on the left, the front is propagating to the right. Parameter values used: $k_1^{f} = 72$, $k_{-1}^{f} = 125.28$, $k_2^{f} = 12.48$, $k_{-2}^{f} = 0.656$, $k_3^{f} = 112$, $k_4^{f} = 3.2$ and $D_A = D_P = 10$, which give the front speed $v_f = 1.627$.

of the reactions between X and Y. The goal is that under $(A, P) = (A_-, P_+)$ conditions, i.e. before arrival of the front, the system has a limit cycle attractor in the (X, Y) plane of phase space and after front passage, for $(A, P) = (A_+, P_-)$, it has two stable stationary states. In the bistable regime, separatrix of the saddle point between the stable states has to cut through the limit cycle of the oscillatory regime, so that, after front passage, concentrations will be switched to one of the steady values depending on the phase of oscillations at the moment of front arrival. To this aim we require that, for $(A, P) = (A_-, P_+)$, one of the stationary states is unstable and surrounded by a limit cycle and for $(A, P) = (A_+, P_-)$, i.e. after front passage, it becomes stable. In addition, its basin of attraction has to be shifted towards higher concentrations of X and Y. The proposed scheme for chemical oscillations is:

$$\mathrm{X} \xrightarrow{k_1} \mathrm{R}, \tag{8}$$

$$2\mathrm{X} + \mathrm{Y} + \mathrm{P} \xrightarrow{k_2} 3\mathrm{X} + \mathrm{P}, \tag{9}$$

$$\mathrm{Y} \xrightarrow{k_3} R, \tag{10}$$

$$\mathrm{R} + \mathrm{A} \xrightarrow{k_{-3}'} \mathrm{Y} + \mathrm{A}. \tag{11}$$

To avoid destruction of the crenel-like spatial structure developing between system origin and arrest front, it is necessary that X and Y molecules are immobile. The reaction rate equations for evolution of the clock are given by:

$$\partial_t X = k_2 X^2 Y P - k_1 X, \tag{12}$$

$$\partial_t Y = -k_2 X^2 Y P - k_3 Y + k_{-3} A, \tag{13}$$

where $k_{-3} = k_{-3}' R$. Note that the reactions associated with the clock given in equations (8)–(11) do not modify the dynamics of species A and P given in equations (5) and (6). Figure 2 gives two sections of the phase space (A, P, X, Y) associated with stationary (A, P) values, (A_-, P_+) and (A_+, P_-). In each section, the intersections $dX/dt = dY/dt = 0$ of the nullclines in the (X, Y)

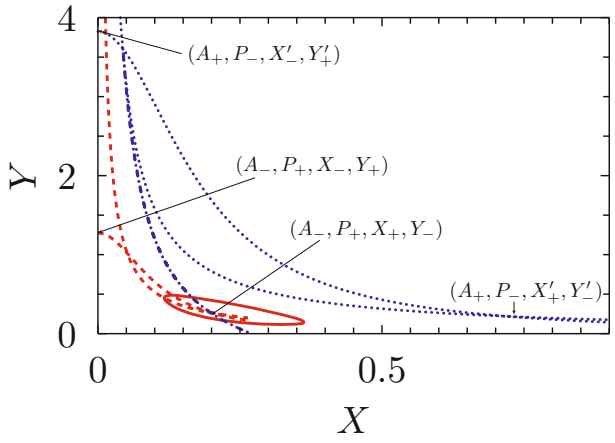

Fig. 2. The X, Y phase space. Projections of nullclines and attractors of the dynamical system obeying equations (5), (6), (12) and (13) onto the (X, Y) space. In the section of the phase space associated with (A_+, P_-), the dotted lines correspond to the nullclines and the dashed-dotted line is the separatrix between the basins of attraction of the two stable steady states $(X'_\pm, Y'_\mp)$. In the section associated with (A_-, P_+), the dashed lines are the nullclines and the solid line is the limit cycle. In both sections, there is also a stable branch at $X = 0$. Parameter values used: $k_1 = 1$, $k_2 = 19/P_+$, $k_3 = 0.2$, $k_{-3} = 0.255/A_-$, where A_- and P_+ are calculated with the parameter values given in Figure 1 caption.

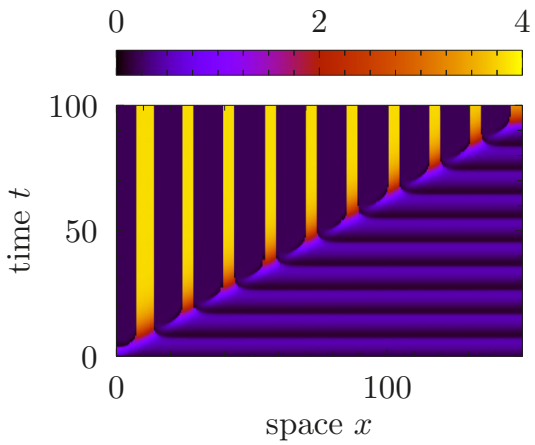

Fig. 3. Deterministic evolution of the system without coupling of oscillations. Space-time (horizontal-vertical) plot of the concentration of species Y (depicted by colour gradation) as calculated from the reaction-diffusion equations (5), (6), (12) and (13).

plane give the steady states of the system. In the (A_-, P_+) section, the system possesses a stable limit cycle and in the (A_+, P_-) section, it is bistable. For the parameters used, the system of equations (5), (6), (12) and (13) possesses a stable node (A_-, P_+, X_-, Y_+), an unstable node-focus (A_-, P_+, X_+, Y_-) surrounded by a stable limit cycle, a stable node (A_+, P_-, X'_-, Y'_+), and a stable node-focus (A_+, P_-, X'_+, Y'_-). If the front is steep and the dynamics given in equations (5) and (6) is faster than the oscillating dynamics given in equations (12) and (13), the state of the system in the (X, Y) plane will not change significantly during the passage from (A_-, P_+) to (A_+, P_-). Under these conditions, the separatrix in the section defined by (A_+, P_-) can be used to cut the limit cycle in the section $(A, P) = (A_-, P_+)$ into two different domains. Position along the limit cycle relative to the separatrix determines further relaxation toward either the stable node, (A_+, P_-, X'_-, Y'_+), or the stable node-focus, (A_+, P_-, X'_+, Y'_-). Hence, evolution of a spatial cell is determined by the phase of oscillation at the moment when this cell is reached by the wave front.

We perform numerical integration of equations (5), (6), (12) and (13) for a one-dimensional system of 300 spatial cells of length 0.5 and volume $V = 4 \times 10^5$ each. Initially, six leftmost cells are in the state (A_+, P_-) and the remaining ones in the state (A_-, P_+). In all cells, concentrations of X and Y are initially equal to $X = 0.25$ and $Y = 0.143$, which corresponds to a point on the limit cycle in the (X, Y) plane. Zero-flux boundary conditions are used.

The results are presented in Figure 3. The wave front propagates with the speed $v \approx 1.59$, in agreement with analytical prediction given by equation (7). Spatial cells ahead of the wave front oscillate in synchrony with a period $T \approx 9.5$ for the values of the parameters used. A periodic structure of alternating X and Y concentrations emerges behind the front. Behavior similar to the clock and wavefront model is reproduced. The first and last segments are deformed due to initial and boundary conditions.

We now examine robustness of the spatial structure to internal fluctuations by studying them at a mesoscopic level. The stochastic description is based on a master equation, which governs time evolution of probability of species populations:

$$\begin{aligned} d_t P(\{S\}, t) = \sum_i \Bigg\{ & \sum_r \left[\omega_r(S_i - z_r) P(S_i - z_r) - \omega_r(S_i) P\right] \\ & + \sum_{\alpha = A, P} \Big[\omega_\alpha(N_\alpha(i) + 1) \\ & \times \Big(P(N_\alpha(i) + 1, N_\alpha(i+1) - 1) \\ & + P(N_\alpha(i-1) - 1, N_\alpha(i) + 1)\Big) \\ & - 2\omega_\alpha(N_\alpha(i)) P\Big] \Bigg\}, \end{aligned} \tag{14}$$

where the vector $S_i = (N_A(i), N_P(i), N_X(i), N_Y(i))$ gives populations of all species in the ith spatial cell, and $\{S\}$ is the collection of vectors S_i in all cells. $\omega_r(S_i)$ is the transition probability of rth reaction, z_r is the vector of population changes caused by rth reaction, and $\omega_\alpha(N_\alpha(i))$ is the transition probability associated with jump by diffusion of α-type molecule from cell i to adjacent cells. Populations $N_\alpha(i)$ and vectors S_i that are the same as on the left hand side were omitted in the argument list of the P function on the right hand side of the master equation. The full list of transition probabilities and vectors

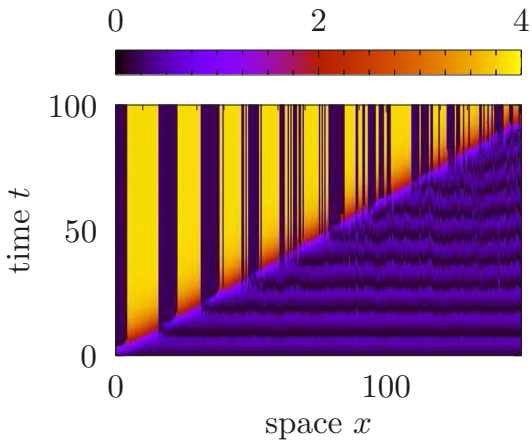

Fig. 4. Stochastic evolution of the system without coupling of oscillations. Same caption as in Figure 3, but for results of the master equation simulation.

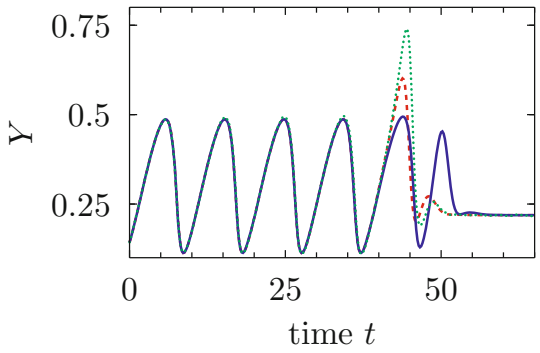

Fig. 5. Evolution of concentration of Y in two example cells for the model given in equations (5), (6), (12) and (13), but with diffusion of X and Y. Results of numerical solution of the deterministic equations are shown for a cell at $x = 73$ (dashed line), which is in a state to the left of the separatrix at moment of front arrival, and a cell at $x = 80$ (solid line), to the right of the separatrix. The dotted line shows results of kinetic Monte Carlo simulations of the master equation for the cell at $x = 73$. Same parameter values as in Figure 2, and $D_X = D_Y = 1$.

z_r is given in the Appendix. We used the kinetic Monte Carlo algorithm proposed by Gillespie to solve this equation [18]. Results of the stochastic approach are presented in Figure 4. The front propagates with a constant velocity, which is not affected by fluctuations. Only first few segments develop normally. Those that are formed later have blurred edges and become indefinable further from the origin. It is a result of desynchronization of oscillations in neighboring spatial cells. Using the two sections of the phase space given in Figure 2, we conclude that, due to fluctuations, the states of spatial cells at front level form a cloud in the (X, Y) plane around the separatrix, leading to random relaxation toward one or the other steady state. Depending on their position, the spatial cells ahead of the front oscillate with different phases and state of the system at the moment when the front passes differs from the deterministic prediction. In this model, which does not include coupling between oscillators, fluctuation-induced desynchronization of oscillations is responsible for segments malformation. This desynchronization is caused by phase diffusion, which does not vanish in unstirred macroscopic systems and is not restricted to an effect of the small number of particles [10,19].

It is worth to note that during segmentation of vertebrate embryos, oscillations in neighboring living cells are believed to be synchronized through the Notch cell-cell signaling pathway [20–22]. A phenotype similar to results shown in Figure 4 was observed in zebrafish embryos with mutations blocking this pathway [23]. When the Notch cell-cell pathway malfunctions, the first somites form normally, but the next ones are irregular.

3 Coupling of oscillators

To ensure synchronization of oscillations in the region ahead of the front, we introduce diffusion of X and Y species, which offers the simplest mechanism of spatial coupling. Synchronization of oscillations is an important issue in dynamics of nonlinear systems [24].

However, as already mentioned, introduction of X and Y diffusion in the model given in equations (5), (6), (12) and (13) destabilizes the periodic pattern behind the wave front. Instead of a spatial structure, the system reaches the homogeneous steady state (A_+, P_-, X'_+, Y'_-). This behaviour is presented in Figure 5, which shows time evolution of Y concentration in two example cells. In spatial cells that are in states located to the right of the separatrix in Figure 2 at the moment of front arrival, expected relaxation toward the steady state (A_+, P_-, X'_+, Y'_-) is observed. States to the left of the separatrix start to evolve toward the low X, high Y steady state as in the system without coupling, but diffusion causes the final relaxation toward (A_+, P_-, X'_+, Y'_-), because (X'_+, Y'_-) is the dominant attractor in the (X, Y) plane. As a result, a transient maximum of Y is observed in Figure 5.

The maximum is higher in stochastic simulations than in deterministic results. This is due to a difference in separation between the A and P fronts in the two approaches. Distance between the inflection points of the antagonistic profiles is 25% bigger in master equation simulations than in deterministic results. Due to larger front separation, the system remains in a transient state of low concentrations of P and A during a longer period of time in kinetic Monte Carlo simulations of the master equation. Under these conditions, the rate of reaction (9) is decreased, while the rate of reaction (11) is not significantly increased with respect to the rates in the (A_-, P_+) state. Then, the limit cycle is shifted and higher values of Y can be reached during this period of time. Only upon arrival of the A front, the basins of attraction recover the same configuration as in Figure 2.

To obtain a stationary spatial structure and synchronization of X and Y oscillations, in addition to the diffusion of X and Y, we introduce an immobile species I, which has bistable dynamics. The final structure should consist of alternating regions in different stable states of I.

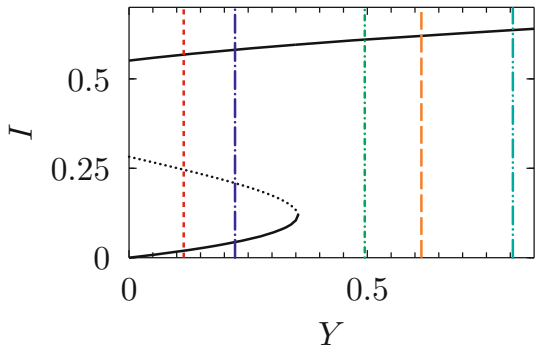

Fig. 6. Bifurcation diagram of species I involved in the mechanism given in equations (15)–(17). Stationary state of I vs. concentration of Y. Solid lines show stable stationary states and the dotted line an unstable stationary state. The dashed and dashed-dotted lines are the minimal and maximal Y values along the limit cycle, respectively. The long-dashed-dotted line is the steady value of Y in the final state (A_+, P_-, X'_+, Y'_-). The long-dashed and long-dashed-double-dotted lines are the highest transient maxima of Y right after front passage obtained from the deterministic and stochastic calculations, respectively. Parameters values are the same as in Figure 5 with additional ones: $k_1^I = 7.03125$, $k_{-1}^I = 8.4375$, $k_2^I = 1.3125$. Initially, $I = 0.0546$.

Such a structure can be stable, only if I molecules do not diffuse. Dynamics of I is inspired from the Schlögl model and admits two stable states. It is coupled to the dynamics of Y according to:

$$2\mathrm{I} + \mathrm{R} \underset{k_{-1}^I}{\overset{k_1^{I'}}{\rightleftarrows}} 3\mathrm{I}, \tag{15}$$

$$\mathrm{I} \xrightarrow{k_2^I} \mathrm{R}, \tag{16}$$

$$\mathrm{Y} \xrightarrow{k_3} \mathrm{I}, \tag{17}$$

where the last reaction replaces equation (10). Adding these reactions does not change the dynamics of species A, P, X nor Y. Before front passage, the system is in the lower I state. The temporal maximum of Y concentration just after front passage works as a switch between the states of I. To get an intuitive picture of I dynamics, we first consider the concentration of Y as a parameter and plot a bifurcation diagram of I in Figure 6. The system given in equations (15)–(17) is bistable for small concentrations of Y and becomes monostable above some threshold. The parameter values $k_{\pm 1}^I$ and k_2^I must be chosen such that the transient maximum of Y is far into the monostable domain, to ensure relaxation of I toward the single high concentration steady state during the short-lived spike of Y. For the values of Y explored on the limit cycle given in Figure 3, the concentration of I has to remain low. On majority of the cycle, I has two stable states, but it is monostable on the remaining part. The dynamics of I is slow enough to prevent transition to high I values during periodic oscillations. This transition only occurs during the spike of Y. The full reaction-diffusion system with coupled oscillators is:

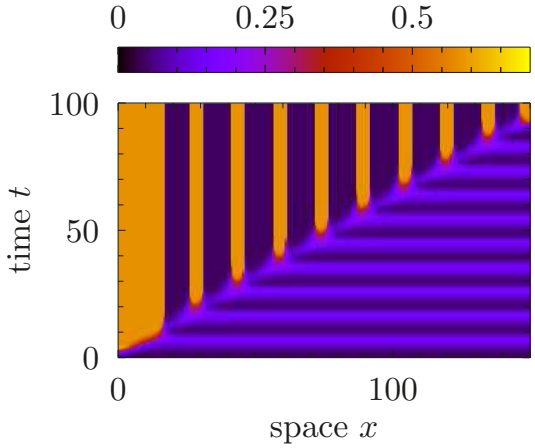

Fig. 7. Deterministic evolution of the system with coupling of oscillations. Space-time plot of concentration of species I (colour gradation) obtained from the numerical integration of the reaction-diffusion equations (18)–(22) for the model with coupled oscillators.

$$\partial_t A = -k_{-1}^f A^3 + k_1^f A^2 - k_2^f A + k_{-2}^f + D_A \partial_{xx} A, \tag{18}$$

$$\partial_t P = -k_3^f AP + k_4^f + D_P \partial_{xx} P, \tag{19}$$

$$\partial_t X = k_2 X^2 YP - k_1 X + D_X \partial_{xx} X, \tag{20}$$

$$\partial_t Y = -k_2 X^2 YP - k_3 Y + k_{-3} A + D_Y \partial_{xx} Y, \tag{21}$$

$$\partial_t I = -k_{-1}^I I^3 + k_1^I I^2 - k_2^I I + k_3 Y, \tag{22}$$

where: $k_1^I = k_1^{I'} R$. For the chosen parameter values, this system admits four stable steady states: two node-focuses $(A_+, P_-, X'_+, Y'_-, I'_-)$ and $(A_+, P_-, X'_+, Y'_-, I'_+)$, and two nodes, $(A_-, P_+, X_-, Y_+, I_0)$ and $(A_+, P_-, X'_-, Y'_+, I'_0)$ In addition, the system possesses two unstable node-focuses $(A_-, P_+, X_+, Y_-, I''_\pm)$ surrounded by stable limit cycles.

Results of numerical integration of the reaction-diffusion equations and of kinetic Monte Carlo simulations of the master equation are shown in Figures 7 and 8, respectively. Contrary to the case without coupling of oscillators, the results of the macroscopic and stochastic approaches are now in qualitative agreement. Fluctuations do not cause desynchronization of oscillations in different cells. The spatial period λ of the developing structure is equal to the distance the front travels during a single period of oscillations. This prediction $\lambda = Tv_f \approx 15$ agrees with the value $\lambda = 14.7$ obtained from the numerical solution of equations (18)–(22), presented in Figure 8. Period of the structure is the same in the deterministic and stochastic simulations. Segments are regular and have well-defined boundaries, but in the kinetic Monte Carlo simulations the regions with high I are wider. This is due to the fact that fluctuations increase the height of the transient maximum of Y, as previously discussed and shown in Figure 5.

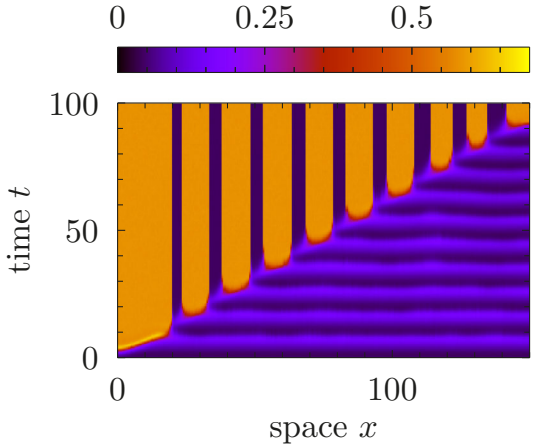

Fig. 8. Stochastic evolution of the system with coupling of oscillations. Same caption as in Figure 7, but for the results of kinetic Monte Carlo simulations of the master equation.

4 Conclusions

We have presented a reaction-diffusion scheme that produces spatial patterns in a way similar to the clock and wavefront model of Cooke and Zeeman. The chemical mechanism consists of three interconnected subsets. The first subset of reactions is associated with bistability for two antagonistic species A and P and propagation of a chemical wave front. The second subset involves two other chemical species X and Y, whose concentrations oscillate and which provide the clock of the model. Reactions between the oscillating species X and Y are coupled to A and P concentrations in such a manner that oscillations are stopped after front passage. Then, the system is driven into a bistable regime with alternating high and low concentrations of X and Y which results in the periodic spatial structure. Oscillations in neighboring cells are coupled through diffusion of X and Y in order to counter fluctuation-induced desynchronization. The last subset of reactions introduces a bistable system for immobile species I that produces the final, stable pattern. Our model entirely relies on reaction and diffusion processes that are defined at the molecular scale, for which the description of internal fluctuations could be made without any additional hypotheses. As a result, the model involving a wave front and a clock without synchronization of oscillations was sensitive to noise. To counter this deffiiency and ensure spatial synchronization of oscillations, we have included diffusion of the oscillating species, which resulted in destabilization of the periodic spatial structure. An immobile supplementary chemical species had to be introduced to stabilize the pattern.

The proposed reaction-diffusion scheme has been inspired by the process of somitogenesis in vertebrates. However, it can be regarded quite generally as a model of formation of spatio-temporal structures in far-from-equilibrium chemical systems, alternative to the well-known Turing pattern mechanism.

Table A.1. List of the vectors, $z_r = (\Delta N_A(i), \Delta N_P(i), \Delta N_X(i), \Delta N_Y(i), \Delta N_I(i))$, of population changes and transition probabilities $\omega_r(S_i)$ associated with the rth reaction, where $S_i = (N_A(i), N_P(i), N_X(i), N_Y(i), N_I(i))$ is an instantaneous state of a cell.

r	z_r	$\omega_r(S_i)$
1	$(1,0,0,0,0)$	$\frac{k_1^f}{V} N_A(N_A-1)$
2	$(-1,0,0,0,0)$	$\frac{k_{-1}^f}{V^2} N_A(N_A-1)(N_A-2)$
3	$(-1,0,0,0,0)$	$k_2^f N_A$
4	$(1,0,0,0,0)$	$k_{-2}^f V$
5	$(0,-1,0,0,0)$	$\frac{k_3^f}{V} N_A N_P$
6	$(0,1,0,0,0)$	$k_4^f V$
7	$(0,0,-1,0,0)$	$k_1 N_X$
8	$(0,0,1,-1,0)$	$\frac{k_2}{V^3} N_X(N_X-1) N_Y N_P$
9	$(0,0,0,-1,1)$	$k_3 N_Y$
10	$(0,0,0,1,0)$	$k_{-3} N_A$
11	$(0,0,0,0,1)$	$\frac{k_1^I}{V} N_I(N_I-1)$
12	$(0,0,0,0,-1)$	$\frac{k_{-1}^I}{V^2} N_I(N_I-1)(N_I-2)$
13	$(0,0,0,0,-1)$	$k_2^I N_I$

The work was realized within the International Ph.D. Projects Program co-financed by the Foundation for Polish Science and the European Regional Development Fund within the Innovative Economy Operational Program "Grants for Innovation". The PICS program between CNRS (France) and PAN (Poland) is acknowledged. P.D. acknowledges the French government for fellowship.

Appendix A: Transition probabilities in the master equation

In the Appendix, we give the expressions of the transition probabilities appearing in the master equation given in equation (14) for the model with coupling of oscillators. The instantaneous state of a system in ith cell is given by:

$$S_i = (N_A(i), N_P(i), N_X(i), N_Y(i), N_I(i)), \qquad (A.1)$$

where $N_\alpha(i)$ is the number of particles of species $\alpha = A, P, X, Y, I$ in the ith spatial cell. Table A.1 gives the transition probabilities $\omega_r(S_i)$ associated with the rth reaction and the corresponding vectors, z_r, of population changes due to the rth reaction. The transition probability $\omega_\alpha(S_i)$ associated with diffusion of species α is given by:

$$\omega_\alpha(S_i) = \frac{D_\alpha}{\Delta x^2} N_\alpha, \qquad \alpha = A, P, X, Y, \qquad (A.2)$$

where Δx is the length of a spatial cell.

References

1. A.M. Turing, Philos. Trans. R. Soc. Lond. Ser. B **237**, 37 (1952)
2. S. Kondo, T. Miura, Science **329**, 1616 (2010)

3. P. Dziekan, A. Lemarchand, B. Nowakowski, J. Chem. Phys. **137**, 074107 (2012)
4. J.D. Murray, *Mathematical Biology: an Introduction* (Springer, New York, 2002)
5. A. Lemarchand, B. Nowakowski, Europhys. Lett. **94**, 48004 (2011)
6. P. Dziekan, L. Signon, B. Nowakowski, A. Lemarchand, J. Chem. Phys. **139**, 114107 (2013)
7. J. Cooke, E.C. Zeeman, J. Theor. Biol. **58**, 455 (1976)
8. M. Kaern, D.G. Míguez, A.P. Muñuzuri, M. Menzinger, Biophys. Chem. **110**, 231 (2004)
9. S.H. Strogatz, Physica D **143**, 1 (2000)
10. M. Malek Mansour, J. Dethier, F. Baras, J. Chem. Phys. **114**, 9265 (2001)
11. L. Herrgen, S. Ares, L.G. Morelli, C. Schröter, F. Jülicher, A.C. Oates, Curr. Biol. **20**, 1244 (2010)
12. F. Baras, Phys. Rev. Lett. **77**, 1398 (1996)
13. J. Dethier, F. Baras, M. Malek Mansour, Europhys. Lett. **42**, 19 (1998)
14. L.M. Pismen, *Patterns and Interfaces in Dissipative Dynamics* (Springer Series in Synergetics, Berlin, Heidelberg, 2006)
15. F. Schlögl, Z. Phys. **253**, 147 (1972)
16. G. Nicolis, I. Prigogine, *Self-organisation in Nonequilibrium Systems* (Wiley, New York, 1977)
17. L.G. Morelli, S. Ares, L. Herrgen, C. Schröter, F. Jülicher, A.C. Oates, HFSP J. **3**, 55 (2009)
18. D.T. Gillespie, Ann. Rev. Phys. Chem. **58**, 35 (2007)
19. A. Fraikin, H. Lemarchand, J. Stat. Phys. **41**, 531 (1985)
20. Y.J. Jiang, B.L. Aeme, L. Smithers, C. Haddon, D. Ish-Horowicz, J. Lewis, Nature **408**, 475 (2000)
21. E.M. Özbudak, J. Lewis, PLoS Genet. **4**, e15 (2008)
22. F. Giudicelli, E.M. Özbudak, G.J. Wright, J. Lewis, PLoS Biol. **5**, 1309 (2007)
23. J. Lewis, E.M. Özbudak, Dev. Dyn. **236**, 1410 (2007)
24. A. Pikovsky, M. Rosenblum, J. Kurths, *Synchronization: a Universal Concept in Nonlinear Sciences* (Cambridge University Press, 2001)